Original Article

Normal Computed Tomography Findings of Head in Lovebird (*Agapornis Roseicollis*)

Maryam Azari[1], Mehdi Rezaei[1*], Siamak Alizadeh[2], Mohammadreza Hosseinchi[3]

1. Department of Clinical Sciences, Faculty of Veterinary Medicine, Urmia Branch, Islamic Azad University, Urmia, Iran.
2. Department of Clinical Sciences, Faculty of Veterinary Medicine, Naghadeh Branch, Islamic Azad University, Naghadeh, Iran.
3. Department of Basic Sciences, Faculty of Veterinary Medicine, Urmia Branch, Islamic Azad University, Urmia, Iran.

Use your device to scan and read the article online

How to Cite This Article Azari, M., Rezaei, M., Alizadeh, S., & Hosseinchi, M. (2025). Normal Computed Tomography Findings of Head in Lovebird (*Agapornis Roseicollis*). *Iranian Journal of Veterinary Medicine, 19*(4), 785-798. http://dx.doi.org/10.32598/ijvm.19.4.1005598

http://dx.doi.org/10.32598/ijvm.19.4.1005598

ABSTRACT

Background: Computed tomography (CT) scanning is one of the most practical and precise diagnostic imaging methods used to evaluate birds' heads.

Objectives: This study aimed to present normal anatomical data of the head of a lovebird (*Agapornis roseicollis*) using the CT method. The features of the bird's head were investigated in terms of bones, joints, muscles, sinuses, and other constituent tissues.

Methods: This current retrospective cross-sectional study included carcasses of six adult lovebirds (*A. roseicollis*) (three males and three females), with an average age of 1–3 years and an average weight of 40–60 g. After preparing the CT images, the head of each parrot was subjected to gross anatomical examination.

Results: Reconstructed CT images identified most structures of the lovebird (*A. roseicollis*) head. The parietal, mandibular, occiput, maxillary, preimaxillary, palatine, pterygoid, quadrate, temporal bones, epithelial membranes, external ear canal and bony labyrinth, ossicles, and entoglossal bones, different parts of the infraorbital sinus, brain hemispheres, and various parts of the eyeball and conchae of the nasal cavities were examined on the CT images. The results related to the CT evaluation and anatomical examination of the lovebird's (*A. roseicollis*) head demonstrated a high correlation.

Conclusion: The study's results can be employed as a reference and a suitable atlas for identifying anatomical features, examining different species of lovebirds (*A. roseicollis*), teaching anatomy, interpreting CT scan images, performing clinical examinations, and treating this type of parrot.

Keywords: Anatomy, Clinical examinations, Computed tomography (CT) scan, Head, Lovebird (*A. roseicollis*)

Article info:
Received: 14 Jun 2024
Accepted: 29 Jul 2024
Publish: 01 Oct 2025

*** Corresponding Author:**
Mehdi Rezaei, PhD.
Address: *Department of Clinical Sciences, Faculty of Veterinary Medicine, Urmia Branch, Islamic Azad University, Urmia, Iran.*
Phone: *+98 (44) 33461732*
E-mail: *Mehdi217mr@yahoo.com*

Copyright © 2025 The Author(s);
This is an open access article distributed under the terms of the Creative Commons Attribution License (CC-By-NC: https://creativecommons.org/licenses/by-nc/4.0/legalcode.en), which permits use, distribution, and reproduction in any medium, provided the original work is properly cited and is not used for commercial purposes.

Introduction

Lovebirds (*Agapornis roseicollis*) with a green body and orange head belong to the order of Psittaciformes, the family of Psittacidae and the genus Agapornis (Silveira et al., 2023; Yaren Kuloğlu & Boydak, 2024). The Brazilian parrot has many names in the Persian language; some call it "dwarf parrot" and some call it "love parrot" or "love bird." The English name of this bird is "lovebird," its German name is "Die Unzertrennlichen" and its French name is "les Inséparables" (Marez, 2003; Salavati et al., 2024). The length of this parrot is between 13-17 cm, and its weight is between 40-60 g (Dueker et al., 2023). The average lifespan of these parrots in captivity is 20-30 years, and it has been reported to be more than 40 years in some cases. The heads of parrots are normally large and comprise approximately 15–20% of the total body weight (Rassouli et al., 2022). The eyes constitute the bulk of the skull and are located inside a sclerotic pupil. In some parrot species, the lower part of the eye is surrounded by a unique bony or suborbital arch (Henley, 2018). The rostrum of the parrot is connected to the skull bone by a joint, which gives the rostrum the ability to move upwards. The parrot tongue is more active and agile due to the entoglossal bones inside its mouth (Benedict et al., 2022). The mandibles and maxillae of these birds are placed inside the upper and lower elements of the beak (Forouzan & Cohen, 2021).

The mandible contains the nasal cavity, inside which turbinates or conchae are stretched longitudinally. Among diagnostic imaging techniques, conchae can only be detected using computed tomography (CT) (Langlois et al., 2021). Parrots have distinct sinuses on their faces. The primary sinus chamber and infraorbital sinus surround the ventral part of the eyeball and extend to areas around the eyes and ears through a series of canals. Some of these canals and the cervicocephalic air sac extend to the central concha, lower jaw and posterior neck. Except for the rostral part of the infraorbital sinus, these sinuses can be examined only using CT or magnetic resonance imaging (MRI) (Pavlova et al., 2021; Mohammed et al., 2022; Faux & Logsdon, 2022). Parrots lack prefrontal, postfrontal, temporal, and postparietal skull bones. The palatal bones of the parrots are small and light. These birds lack teeth and have a large and ossified brain chamber, which leads to weight loss and ease of flight (Carril et al., 2021; Hollwarth et al., 2023; Salehi et al., 2024). Parrots kept at home and able to fly may suffer head injuries under certain conditions. For instance, a bird may hit a window or land in an inappropriate place, which leads to traumatic injuries. Various imaging techniques can be used to diagnose these types of damages. Currently, CT is one of the most accurate and practical diagnostic imaging methods that can be employed to evaluate head diseases in birds. Veladiano et al. (2018) examined the natural anatomy of the heads of blue-and-yellow macaws (*Ara ararauna*), African gray (*Psittacus erithacus*) and monks (*Myiopsitta monachus*) by CT, labeled different parts of their heads on CT images, and finally introduced the obtained findings as an atlas of the natural head anatomy of these parrots. Similarly, using the CT method, Faillace et al. (2021) investigated the anatomical features of the head of the blue-fronted Amazon parrot (*Amazona aestiva*). According to this research, some of these features, such as the size and position of the nasal conchae, infraorbital sinus chamber, nasopharyngeal duct, and paraglossum, were different in this type of parrot compared to other parrots, which can be used in anatomical analysis. They also reported that the inner ear, its related structures, and the paratympanic sinus cannot be well examined in normal CT images of this type of parrot. Similarly, Thurber et al. (2015) evaluated the differential diagnosis of parrots' neurological symptoms caused by hydrocephalus syndrome. They concluded that CT is a suitable screening tool for diagnosing hydrocephalus in this sick bird. In addition, using potassium iodide contrast medium and CT imaging, Jones et al (2019). Investigated the radioanatomical characteristics of the rock dove or the common pigeon, especially in the head. They found that CT scanning can be utilized as a preferred method for examining different body tissues of this type of bird, and the images obtained using this method will be a valuable source for clinical applications and educational and research purposes.

Using CT, Duymus et al. (2013) compared the head anatomy of white, brown and wild *Japanese quails* in terms of head volume, brain volume, parietooccipital air space volume, and calvarial bone volume, and indicated that the head of white quails had the lowest volume values, which was due to genetic differences. Several studies have demonstrated the diagnostic value of CT in the diagnosis of complications and disorders of the parrot head. Hébert (2019) confirmed rostroparasphenopalatal luxation in a red-crowned parakeet (*Cyanoramphus novaezelandiae*) using the CT method, and the bird completely recovered after therapeutic measures. Krautwald-Junghanns et al (1998) compared radiology and CT scan techniques in the diagnosis of head diseases in sick parrots and reported the superiority of the CT method in the diagnosis of complications, such as fractures of the head bones and identification of hypercalcification or hypocalcification and carcinoma in this area. Investigation of

the tomographic features of the head of the rose-ringed parakeet can be beneficial in identifying anatomical features and evaluating pathological cases. However, a precise examination of the details related to the normal anatomy (morphology and morphometry) of different parts of the bird's head is necessary. Radioanatomical studies of the head of the lovebird (*A. roseicollis*) are rare, and there are no detailed reports in this respect. Accordingly, this study aimed to investigate the normal anatomy of the lovebird (*A. roseicollis*) head using three-dimensional (3D) modeling. CT evaluation and anatomical examination of birds will provide valuable findings. The results of this research can be used as a reference and atlas to identify anatomical characteristics, investigate different species of lovebird parakeets, teach anatomical sciences, interpret CT scan images and conduct clinical examinations and treatment of this type of parrot.

Materials and Methods

Study design and birds

The current retrospective cross-sectional study used carcasses of six adult lovebirds (*A. roseicollis*) (three males and three females), with an average age of 1–3 years and an average weight of 40–60 g, who were well fed during their lifetime. Carcasses were obtained from a private breeding center for lovebird parrots in Tehran Province, Iran, then frozen and stored at -20 ˚C. Parrots that had previously died for various reasons were used in this study and the cause of their deaths was unrelated to this study. The maturity of these parrots was confirmed based on factors, such as the type of color of the neck ring, number of scales on the feet, condition of the feathers, and color of the beak. The sex of the parrot was also determined following a necropsy of the carcass (Webb & Gaston, 2000; Vučićević et al., 2016).

CT study

To prepare the CT images, the lovebird (*A. roseicollis*) was placed on the CT scan table in a sternal recumbent position, and the head of the bird was kept facing forward so that its mandible was perpendicular to the gantry. Head scans were performed in the sagittal, transverse, and dorsal planes, with a thickness and interval of 1 mm. A helical scanner (Toshiba Multi-slice CT Scanner Asteion Premium 4: TSX-021B, Japan) was used for CT. In addition, appropriate windows were selected to examine soft and bone tissues. The technical factors of the CT scanner included gantry rotation time (400 ms), slice thickness (1 mm), reconstruction distance (0.5–1 mm), pitch ratio (1), kVp (120), mAs (10), physical detector collimation (32×0.6 mm), final section collimation (64×0.6 mm), resolution (512×512 pixels), resolution range (0.92×0.92), kernel (10 H), and increment (0.5 mm) (Ma et al., 2021; Faillace et al., 2021). Imaging was performed based on the factors mentioned above, and the obtained images were saved in DICOM format (Brühschwein et al., 2018).

3D reconstruction

After saving the obtained images in the DICOM format, they were transferred to a computer loaded with 3D modeling software (Onis CT software, Multi-Modality Workplace: VE 2.5A) and displayed using bone window settings (window width: UH 4500 and window level: UH750), according to previous research (Wilhite & Wölfel, 2019). Next, these images were analyzed using 3D slicer software (Šljivic et al., 2019). Based on our observations, this technique allowed the use of lung (WW: 2336 HU; WL: 368 HU) and bone (WW: 950; WL: 390) windows, thus providing high-resolution images of the tissues and structures that constitute the head of the parrots.

Anatomical study

After preparing the CT images, the heads of each frozen parrot were transversely cut with an electric band saw at intervals of 5 mm from the rostral part of the rhamphotheca to the anterior end of the neck. Each prepared slice was cleansed with water and a soft brush and photographed. Visible textures and structures were identified and labeled in these photographs. Furthermore, the CT images matched these photos and were labeled accordingly. Nomina Anatomica Veterinaria was used as the scientific term (Veterinaria, 2017) (Figures 1 and 2).

Results

Based on these results, most structures of the head of the lovebird (*A. roseicollis*) were detected using reconstructed CT images. In the 3D images, the head of the parrot is round and compact. The jugal arch and palatine bone were fused in the remaining parts of the skull, except for the bones of the cranial parts of the face. Small head bones, such as the ear and entoglossal bones inside the mouth, can also be evaluated in these CT images. In this study, it was possible to observe bony trabeculae in the head of this type of parrot using the lung window. In addition, the parietal and temporal bones, nasal conchae, epithelial membranes, external ear canal, and bony labyrinth were examined using this filter. Furthermore, by covering tissues, different parts of the

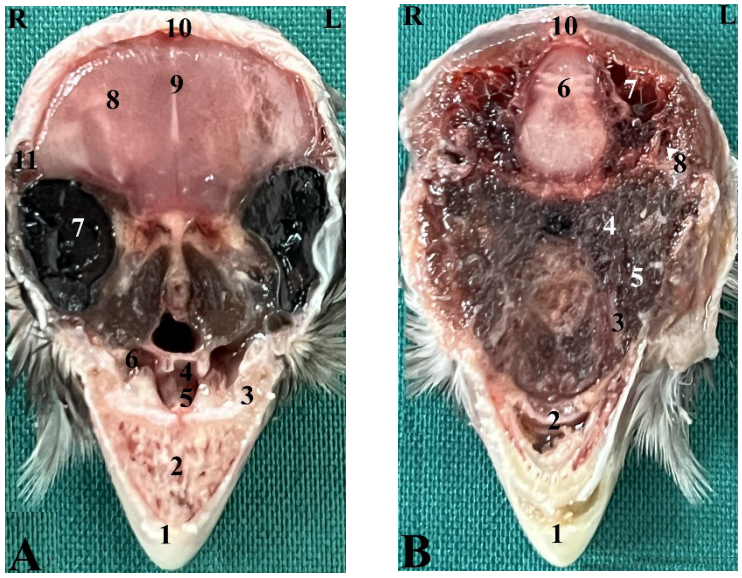

Figure 1. Representative photographs of anatomic cross sections of the adult lovebird's (*A. roseicollis*) head

A) Level of the eye, B) Level of the external acoustic meatus in the dorsal plane; A: 1) Ramphoteca, 2) Premaxilla bone, 3) Maxilla bone, 4) Left nasal cavity, 5) Caudal nasal concha, 6) Infraorbital sinus, 7) Eye, 8) Brain hemispheres, 9) Falx cerebri, 10) Occipital bone, 11) Temporal bone, B: 1) Ramphoteca, 2) Premaxilla bone, 3) Palatine bone, 4) Ethmomandibularis muscle, 5) Pterygoideus muscle, 6) Cerebellum, 7) Bony labyrinth, 8) External acoustic meatus, 9) Caudal nasal concha, 10) Occipital bone.

infraorbital sinus could be observed using this window. Furthermore, different soft tissue windows were adjusted to identify the brain hemispheres, cerebellum, optic nerve, pupil muscles, and eye lenses (Figures 3, 4 and 5). Based on these results, the columella ossicle, external cartilage, and cochlea were undetectable on

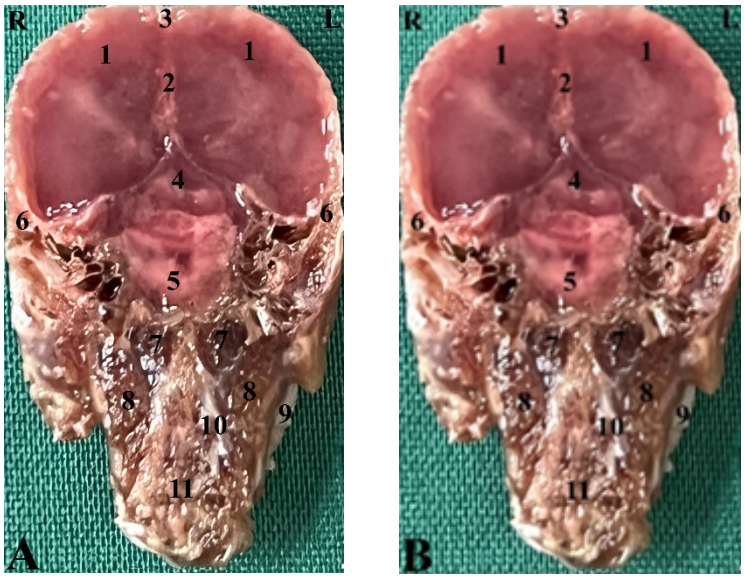

Figure 2. Representative photographs of anatomic cross sections of the adult lovebird's (*A. roseicollis*) head

A) Level of the rostral border of the orbital fossa, B) Level of the external acoustic meatus in the transverse plane; A: 1) Frontoparietal bone, 2) Eye, 3) Infraoebital sinus, 4) Pterygoideus muscle, 5) Ethmomandibularis muscle, 6) Hard palate, 7) Eye, 8) Caudal nasal concha, 9) Lingual process of hyoid bone, 10) Tongue, 11) Choanal cleft, 12) Mandible, B: 1) Cerebrum, 2) Falx cerebri, 3) Occipital bone, 4) Brain stem, 5) Chiasma optic, 6) External acoustic meatus, 7) Ethmomandibularis muscle, 8) Pterygoideus muscle, 9) Mandible, 10) Hard palate, 11) Lingual process of hyoid bone.

R: Right; L: Left.

the CT images. The parrots' eyeballs were complete, bony, and located on the skull's lateral side (Figure 3i). The mandible was bony and lacked a distinct symphysis (Figures 3b and 4a). The rostrum was keratinous, large, and curved ventrally. Moreover, the operculum was identified in the dorsal part of the nostrils (dorsal base of the nose). The occipital, maxillary, premaxillary, mandibular, palatine, pterygoid, and quadrate bones were pneumonized and had air bubbles. The nasal cavity was separated using a septum. The thickness of this septum increased slightly from the rostral to the caudal side. The caudal third of this septum was cartilaginous, and the middle third and rostral parts were bony. The ectethmoid, mesethmoid, maxillary, and preimaxillary bones were involved in the nasal cavity formation. The nasal cavity had olfactory, respiratory, and vestibular components. Each nasal cavity had a single duct with the caudal, middle, and rostral cartilaginous conchae. The rostral concha was C-shaped and was located on the vestibular part of the nasal cavity. The thickness of this concha decreased from the rostral to the caudal direction. The rostral concha contained a basal lamella and was located on the lateral wall of the nasal cavity. The middle concha was in the form of long ducts that originated from the basal lamella and were located in the upper respiratory tract of the nasal cavity. This lamella splits into sinusoidal and spiral lamellae. This spiral lamella extended to the entrance of the nasopharyngeal canal. The caudal concha was small and hollow and was located in the caudal part of the nasal cavity. The nasal and oral cavities were connected via the nasopharyngeal canal (Figures 4c and 5h).

The nasopharyngeal duct was connected to the maxillary palatal process and choanal part of the palatine bone from the rostrolateral and caudal sides, respectively. The caudal part of the nasopharyngeal duct was linked to the interorbital septum (Figures 4e and 5f). The oral cavity consists of palatal, mandibular, premaxillary, and maxillary bones, as well as their related muscles and tongue. These oral bones and the pterygoid also play a role in the pharynx formation (Figures 5c and 5d). The choana was located in the dorsal part of the pharynx and oral cavity and connected the oral cavity to the nasal cavity (Figure 3g). The strong and large tongue of the lovebird (*A. roseicollis*) could be identified in the CT images, which was located in the caudal and middle third of the inferior part of the oral cavity (Figures 3c and 3d). The oral cavity contained a hyobranchial apparatus. The base of the tongue was in close contact with the paraglossum and cranial part of the basihyal. Bishyal processes and uhorial bones were detectable in the trachea's larynx and cranial part. The branchial horn (the caudal part of the hyobranchial apparatus) was located in the inner part of the ramus of the mandible or the cranial part of the trachea. The caudal third of the branchial horn was related to the mandibular masseter muscle. The larynx consists of a ring-shaped cricoid cartilage and two pyramid-shaped arytenoid cartilages. The results of the current study demonstrated that the procricoid cartilage was located in the middle of the cricoid cartilage and formed the dorsocaudal part of the larynx (Figures 3b, 3c, 3d, 3e, 3f, 3g, 3h, 3i and 3j). The glottis was located in the central part of the larynx and was surrounded by arytenoid cartilage. Laryngeal mounds (*Mons laryngealis*) were detected on the cross-sectional CT images. The location where the cricoid joins the tracheal cartilage was found to be ring-shaped in these images (Figures 3f and 5f).

The entire pupil cavity was filled with an oval eyeball. The frontal bone and suborbital arch form the outer edges of the eyeball. Trabecular bony septum was observed between the pupils of the eyes. All parrots under study had a complete bony eyeball (Figures 3j and 5h). In the obtained CT images, the eye lens was not detectable, and the cranial chamber (aqueous) and caudal chamber (vitreous) were not distinguishable. The retina was unrecognizable. The eyeball muscles, lacrimal glands, and third eyelid (nictitating membrane) showed the same attenuation and could not be separated from each other. The scleral bones were found as two indistinct lines in the cross-sectional images and circular or round in the sagittal images (Figures 3j, 4a and 5h).

The encephalon of a lovebird (*A. roseicollis*) was evaluated using CT images (Figures 4c and 5i). In cadaver samples, brain hemispheres, such as the telencephalon and diencephalon, as well as the brainstem and cerebellum, were detectable and could be distinguished. However, these structures had similar attenuation in the CT images, and their distinction was difficult. The results revealed that the external acoustic meatus and the external opening of the ear of the lovebird parakeet could be recognized in the CT images (Figures 3m and 5c). Identifying the tympanic membrane in these birds' CT images and carcasses was impossible. Hence, different parts of the middle ear were not distinguishable. Nonetheless, low-resolution lines in the distal third of the external acoustic meatus can demonstrate parts of the middle ear, such as the infraorbital (columella) and extracolumella cartilage. The bony labyrinth of the inner ear was well-recognized in the cadaver and CT images.

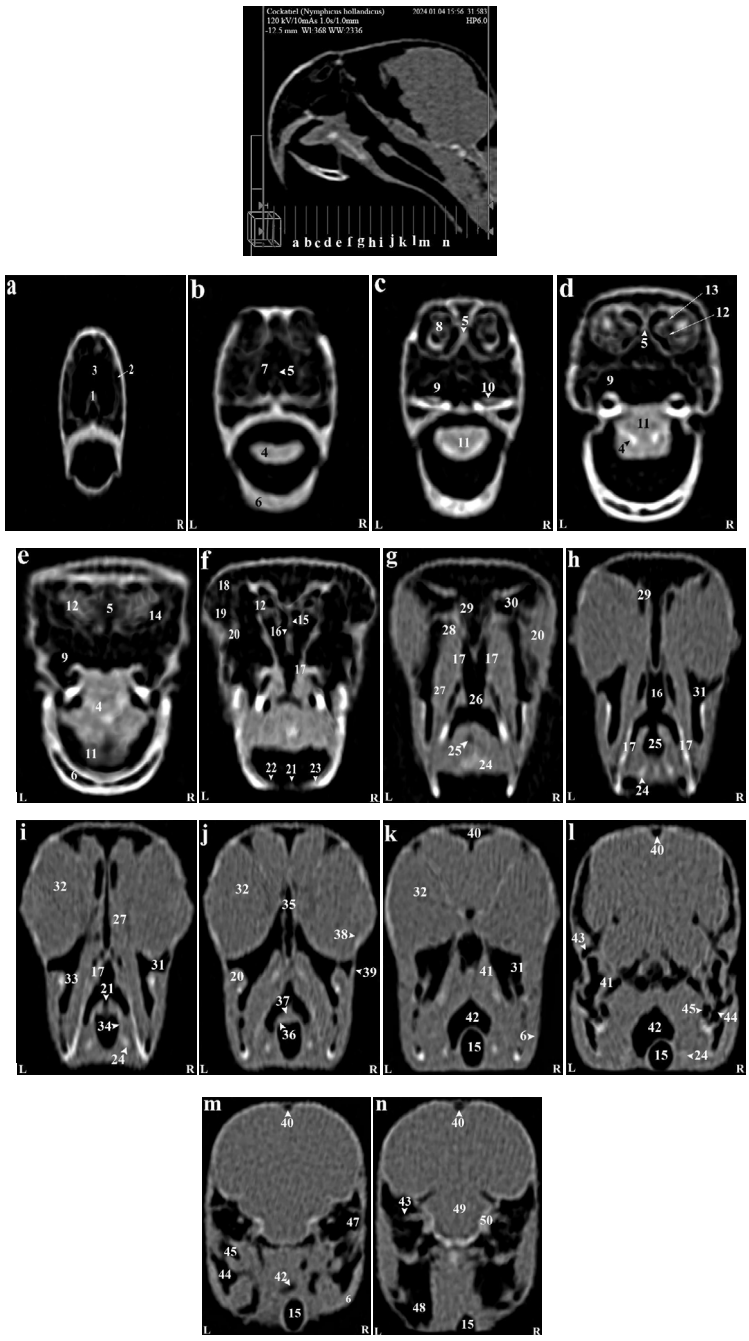

Figure 3. (a-n) Transverse CT reconstruction images in the lateral plane of the normal skull of the lovebird (*A. roseicollis*)

1) Rostral diverticulum septum, 2) Premaxillary bone, 3) Rostral diverticulum, 4) Paraglossum, 5) Bony part of nasal septum, 6) Mandible bone (pneumonized), 7) Palate bone opening, 8) Rostral nasal concha, 9) Transverse canal, 10) Maxillary process of palatal bone, 11) Tongue, 12) Middle nasal turbinate, 13) Basal layer of middle nasal turbinate, 14) Nasal cavity, 15) Cartilaginous part of nasal septum, 16) Nasopharyngeal airway, 17) Lateral border of palatine bone, 18) Periorbital process of infraorbital sinus, 19) Jugal part of infraorbital sinus, 20) Jugal arch, 21) Glottis, 22) Laryngeal protrusion, 23) Arytenoid cartilages, 24) Bronchial horn, 25) Trachea, 26) Choana of palatal bone, 27) Ethmomandibular muscle, 28) Periorbital part of the infraorbital sinus, 29) Caudal nasal turbinate, 30) Infraorbital sinus foramen, 31) Infraorbital part of the infraorbital sinus, 32) Eyeball, 33) Epithelial membrane, 34) Tracheal cartilage ring, 35) Infraorbital septum, 36) Cricoid cartilage, 37) Procricoid cartilage, 38) Scleral ossicles, 39) Suborbital arch, 40) Frontal bone (pneumonized), 41) Pterygoid and quadrate muscles, 42) Larynx, 43) Zygomatic process of the squamosal bone, 44) Quadrate bone (pneumatized), 45) Quadrature part of infraorbital sinus, 46) Postorbital part of infraorbital sinus, 47) External acoustic meatus, 48) Cervicocephalic diverticulum, 49) Brain stem, 50) Bony labyrinth.

L: Left; R: Right.

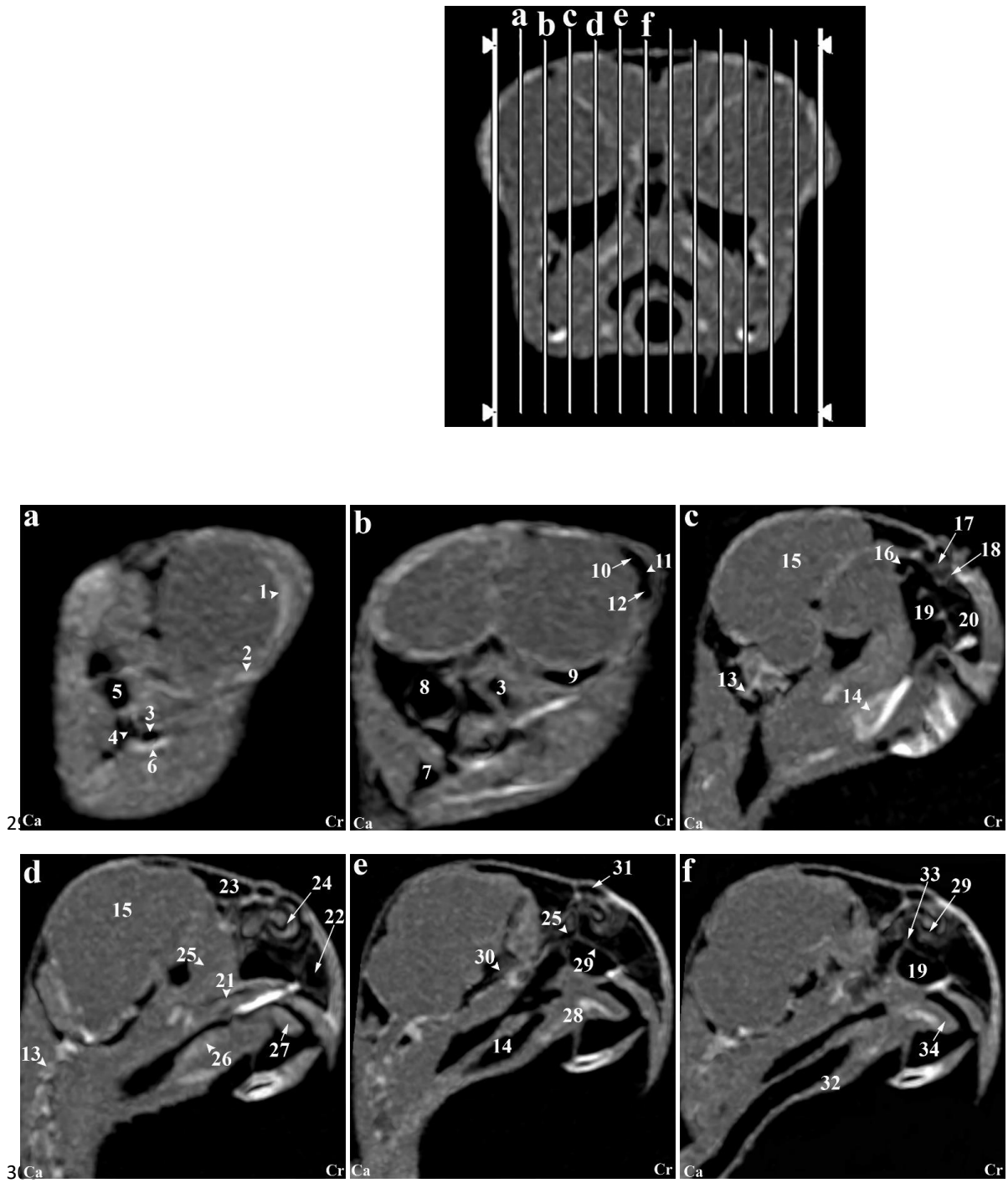

Figure 4. (a-f) Sagittal CT reconstruction images (lateromedial plane) of the normal skull of the lovebird (*A. roseicollis*)

1) Scleral bones, 2) Suborbital arch, 3) Postorbital part of the infraorbital sinus, 4) Quadrate bone (pneumonized), 5) External ear foramen, 6) Mandible bone, 7) Cervicocephalic diverticulum, 8) Occipital bones (pneumonized), 9) Infraorbital part of infraorbital sinus, 10) Periorbital process, 11) Epithelial membrane, 12) Jugal portion of infraorbital sinus, 13) Cervical vertebrae, 14) Trachea, 15) Encephalon of the brain, 16) Caudal nasal turbinate, 17) Middle nasal turbinate, (18) Rostral nasal turbinate, 19) Transverse canal, 20) Premaxillary bone (pneumonized), 21) Palate bone (pneumonized), 22) Rostral diverticulum, 23) Frontal bone (pneumonized), 24) Nasal cavity, 25) Nasopharyngeal airway, 26) Larynx, 27) Paraglossum, 28) Basihyal, 29) Bony part of nasal septum, 30) Infraorbital septum, 31) Nostril, 32) Tracheal rings, 33) Cartilaginous part of nasal septum, 34) Tongue.

Ca: Caudal; Cr: Cranial

Based on our results, the paratympanic sinus could not be detected on CT images. The muscles of the head were hyperattenuated lines and were unclear. Nonetheless, relatively larger muscles, such as the quadrate, pterygoid, and ethmomandibular muscles were distinguishable. Although the jaw adductor muscle is large, it was not detectable on the CT images (Figures 3g and 5c). The infraorbital sinus was surrounded by skull bones and muscular tissues and was found to be a large triangular cavity that covered a large part of the head. The premaxillary bone was located in the rostral part of the sinus. In addition, the palatine and pterygoid bones were located in their inner parts. The quadrate, jugal arch and mandibular bones were located in the lateral part. This sinus included the rostral diverticulum, transverse canal, postorbital, preorbital, infraorbital, quadrate bones, cervicocephalic diverticulum, and mandibular recess. The rostral diverticulum and transverse canal were single and the remaining parts were paired. Except for the periorbital parts, transverse canal, and rostral diverticulum, the remaining parts of the suborbital sinus were covered by the masticatory muscle (Figures 3, 4 and 5). The rostral diverticulum extended along the preimaxillary bone. The diverticulum was divided into two parts by a narrow bony septum. The thickness of this septum decreased from the rostral to the caudal direction; therefore, it completely disappeared in the middle parts of the diverticulum. The transverse channel was visible as a short horizontal channel. The maxillary process of the palatine bone and the maxillary jaw-palatine process (maxillopalatine) of the maxillary bone were located in this canal's ventral and distal parts. The transverse canal connected the periorbital region and rostral diverticulum (Figures 3a, 4d and 5h).

The nasopharyngeal duct divides the periorbital region into left and right parts. The jugal portion was connected dorsally to the periorbital region, ventrally to the choanal part of the palatine bone, and laterally to the jugal arch. A relatively thin epithelial layer separated the periorbital region from the jugal region. These subdivisions were connected to the caudal part and located near the infraorbital part of the infraorbital sinus. The infraorbital region was the largest part of the sinus. It covered a large area of the ventral sinus surface and extended to the eyeball. This part was connected to the palatine bone and interorbital septum from the medial part and the suborbital and jugal arches from the lateral part. The infraorbital and postorbital parts were directly connected. The infraorbital and postorbital regions were the largest parts of the infraorbital sinus. The postorbital part was located in the pterygoid's lateral part, the zygomatic process's internal part, and the jugal bow's posterior part, which was connected to the musculature. The masseter, pterygoid, quadrate and temporal muscles were located in the postorbital area. The caudoventral part of the postorbital was connected to the quadrate portion. The smallest part of the infraorbital sinus was related to the quadrate part, which was laterally connected with the quadrate bone. The mandibular recess and cervicocephalic diverticulum were linked to the postorbital region. The mandibular recess was visible in the inner and rostral parts of the mandibular ramus. This recess was located in the inner part of the postorbital and ventral parts of the infraorbital canal. Based on these results, a cervicocephalic diverticulum was detectable in the skull of the lovebird (*A. roseicollis*) and extended to the neck (Figures 3n and 4b).

Discussion

Based on the CT and gross anatomy results, the skull of the lovebird (*A. roseicollis*) was similar to that of other parrots, and no difference was observed between the skulls of male and female parrots. The CT diagnostic method enabled anatomical description of the skull of the lovebird (*A. roseicollis*), which is consistent with the reports of some researchers in this field (e.g. Sabat et al., 2017; Iwaniuk et al., 2004). Although the heads of these parrots were small, the quality and clarity required to identify the bones and tissues of the head, such as the jugal arch, palatine bone, ear ossicles and antoglossum bones inside the mouth and different parts of the infraorbital sinus, were provided in the obtained CT images. Of course, the type of CT scanner employed in this study (Toshiba Multi-slice CT scanner Asteion Premium 4, Model: TSX-021B, Japan) played an essential role in the quality and resolution of the obtained images, and this device obtained appropriate images of the heads of these parrots. In this study, the bony trabeculae of the head of the rose-ringed parakeet were observed using a suitable window (WW: 2336 HU; WL: 368 HU). The parietal and temporal bones, nasal conchae, epithelial membranes, external acoustic meatus, and bony labyrinth were also identified. Head CT was performed in the sagittal, transverse, and dorsal planes, and images of different tissues of the head, especially various parts of the infraorbital sinus, had diagnostic value. Scanning the head in different planes solved the problem of superimposition of images of different tissues, and each tissue was individually and specifically evaluated accordingly. Cubo and Casinos (2000) examined the bones of different bird species and reported that some birds' bones contain air bubbles, which conforms to the results of our study. Based on our observations, some of the bones related to the skull of the lovebird (*A. roseicollis*), such as the occipital, max-

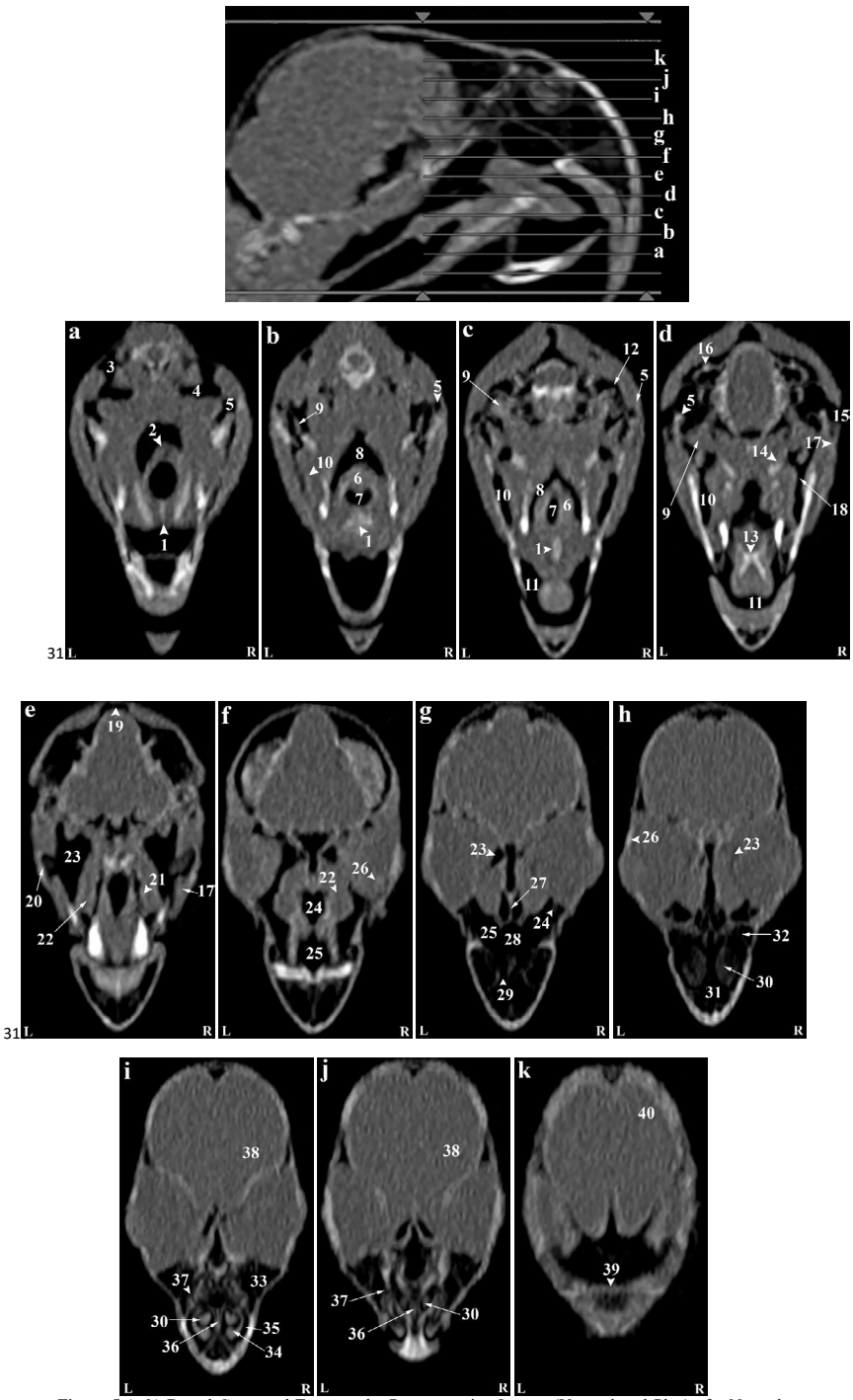

Figure 5. (a-k) Dorsal CT reconstruction images (ventrodorsal plan) of a normal skull of the lovebird (*A. roseicollis*)

1) Basihyal, 2) Arytenoid cartilage, 3) Quadrature part of infraorbital sinus, 4) Epithelial membrane, 5) Quadrate bone, 6) Larynx, 7) Glottis, 8) Pharynx, 9) Pterygoid and quadrate muscle, 10) Mandibular appendage, 11) Oral cavity, 12) External acoustic meatus, 13) Paraglossum, 14) Pterygoid bone, 15) External ear foramen, 16) Bony labyrinth, 17) Jugal arch, 18) Postorbital part of infraorbital sinus, 19) Occipital bones (pneumonized), 20) Suborbital arch, 21) Palate bone, 22) Ethmomandibular muscle, (23) Infraorbital Part of the Infraorbital Sinus, (24) Nasopharyngeal Canal, (26) Scleral Ossicles, (27) Infraorbital Septum, (28) cartilaginous part of the nasal septum, 29) Palate foramen, 30) Middle nasal turbinate, 31) Rostral diverticulum, 32) Cranial foramen of eyeball, 33) Preorbital part of the infraorbital sinus, 34) Rostral nasal turbinate, 35) Nasal cavity, 36) Bony part of nasal sinus, 37) Infraorbital sinus foramen, 38) Encephalon, 39) Craniofacial flexion, 40) Frontal bone.

L: Left; R: Right.

illary, premaxillary, mandible, palatine, pterygoid, and quadrate bones, are trabecular and pneumonia, and have air bubbles. In another study, Veladiano et al. (2018) investigated the head CT of different birds and described the role of the pneumatic foramen, suborbital, and paratympanic sinuses, which contradicts our observations. Based on the CT images of the head of the lovebird (*A. roseicollis*), the pneumatic foramen was undetectable, and the origin of pneumatization of the head bones could not be evaluated. Furthermore, the paratympanic sinus could not be detected in these images, probably due to the fusion of this sinus with the middle ear tissues.

In this study, the tympanic membrane and different parts of the middle ear were not detected on the CT images. However, low-resolution lines in the distal third of the external acoustic meatus can demonstrate parts of the middle ear, such as the columella and extracolumella cartilage. These results corroborate those reported by Wild et al.'s (2015) study. In this study, it has been reported that the cochlea, tympanic membrane, extracolumella cartilage, and columella of parrots are extremely small and thus cannot be observed on CT images. Nonetheless, other diagnostic imaging methods, such as micro-CT or MRI, can be used to evaluate these aspects.

Some studies have indicated the presence of three conchae in the nasal cavities of birds (Isabelle et al., 2020; Hanafy et al., 2021), which is consistent with our study's results. The results of the current study revealed that each nasal cavity of the lovebird (*A. roseicollis*) consisted of a single meatus with caudal, middle, and rostral cartilaginous conchae. Nevertheless, some other studies reported two conchae in the Congo gray parrot (*P. erithacus*) (Pohlemeyer & Kummerfeld, 1989), the budgerigar (*Melopsittacus undulates*) (Orosz, 2016), and the brown-eared nightingale (*Hysipetes amaurotis*) (Yokosuka et al., 2009), or more than three conchae in the petrel (*Pagodroma* sp.) (Piro & Acosta, 2019). In the nostrils of the lovebird (*A. roseicollis*), the middle and caudal turbinates had the largest and smallest sizes, respectively, which conforms to the results of studies conducted by Hanafy (2021) and Al-Rubaie & Kadhim (2023). In the skull of the lovebird (*A. roseicollis*), similar to other parrots, there is a middle concha in the form of a long duct, which is located in the upper respiratory airway and originates from a basal lamella divided into a sinus lamella and a spiral lamella. Moreover, in this type of bird, the caudal concha is small, hollow, and placed in the caudal nasal cavity. However, the results of some studies contradict our observations. Faillace et al. (2021) examined the CT results of the nasal conchae of the blue-fronted Amazon parrot (*A. aestiva*), which indicated that the middle concha is a narrow linear structure inside the rostral concha. They further found that in this type of parrot, the caudal concha can have different sizes, such that the size of this concha is large in some of these birds, while it is extremely small in others. Madkour (2019) claimed that the nasal conchae of some bird species have bone tissue in addition to cartilaginous tissue. This recent report does not match the results of our study because, according to our observations, the structure of the nasal conchae of the lovebird (*A. roseicollis*) was purely cartilaginous, and this result was confirmed by attenuation of the CT images of the head. In another study, Van Zeeland (2018) investigated the upper respiratory tracts of parrots and reported that the nasopharynx is where the nasal cavities connect to the throat and adenoids and most of the lymph tissues are located in this region. The findings of this study are consistent with our gross anatomical results. The nasal and oral cavities were linked through the nasopharyngeal duct of a lovebird (*A. roseicollis*). Based on the CT images, the nasopharyngeal duct was rostrolaterally and caudally connected to the maxilla-palatal process of the maxillary bone and the choanal part of the palatine bone, respectively. The caudal part of the nasopharyngeal duct was associated with the interorbital septum. Unfortunately, it was impossible to find valid studies on the nasopharyngeal CT characteristics of birds and compare their results with those of this study. We hope that the findings of this study will pave the way for future research in this respect.

The oral cavity of the lovebird (*A. roseicollis*) had a hyobranchial apparatus. The caudal part of this system was located in the inner part of the mandibular ramus, or the cranial part of the trachea. These results concur with those of other studies on parrots. According to our observations, the base of the tongue was in close contact with the paraglossum and the cranial part of the basihyal.

The results of the present study demonstrated that the pupil of the lovebird (*A. roseicollis*) is completely bony. In gross anatomy studies, it was possible to determine the cranial and caudal chambers, lens and optic nerve of this bird's eye, which matches the reports of most researchers, and it seems that the eye anatomy of this type of parrot does not differ from that of other birds (Moore et al., 2022). However, unlike the gross anatomical evaluations, the lens was not visible and it was impossible to distinguish the ocular chambers in the obtained CT images. The retina was unrecognizable. The muscles of the eyeball, lacrimal glands, and third eyelid (nictitating membrane) had the same attenuation and, therefore, could not be separated from each other. The researchers of this study could not find written and specific reports

about CT scans of bird eyes or compare them with the results of this study. However, according to the findings of this study, diagnostic imaging methods, such as ultrasonography, micro-CT, MRI and other specialized eye evaluation methods can be used to examine the internal tissues of the eye.

Due to its large size, the masticatory muscle could be identified in CT images obtained from the head of this type of parrot. However, other head muscles, eyeball muscles, and even nerve vessels had very close attenuation, making it difficult to distinguish between them; thus, they did not undergo separate investigations. Different radiation factors were employed to increase the clarity and contrast of these tissues; however, no suitable answers were obtained in this regard.

Based on anatomical examination of the budgerigar and Casco (African grey parrot), Smallwood (2014) reported that the cricoid cartilage of the larynx of these birds is wide and has a rostral process. In another study, Silva et al. (2020) found that the cricoid cartilage of the larynx of the lovebird is smooth and small, and has two rostral and lateral processes, which contradicts our results. In the lovebird (*A. roseicollis*), the larynx consisted of an annular cricoid cartilage and two pyramidal arytenoid cartilages. The cricoid cartilage was smooth, thin, and had no processes. In the middle part of the cricoid cartilage, procricoid cartilage forms the dorsocaudal part of the larynx.

Previous studies have described the anatomy of the infraorbital sinus in some domestic birds, such as hens, turkeys, and geese (Casteleyn et al., 2018). However, no detailed and comprehensive report has been published on the anatomy and CT features of the infraorbital sinus in the parrots. Based on the results of our study, the infraorbital sinus of the lovebird (*A. roseicollis*) was surrounded by skull bones and covering and muscular tissues. The CT images detected it as a large triangular cavity covering a large part of the head. The premaxillary bone was located in the rostral part of the sinus. In addition, the palatine and pterygoid bones were located in the inner part, and the quadrate, jugal arch, and mandible bones were located in the lateral part. Grist (2006) conducted an anatomical study on domestic chickens and found fewer infraorbital sinus chambers in the head of this type of bird. The names and characteristics of these chambers were not mentioned in this report. Eventually, it was indicated that this sinus is shorter in other birds and limited by the infraorbital region. According to our observations, this sinus included the rostral diverticulum, transverse canal, postorbital, preorbital, infraorbital, and quadrate parts, cervicocephalic diverticulum, and mandibular recess in the lovebird (*A. roseicollis*). The head and neck of this type of parrot were widely pneumatized by this sinus. No specific homologies were inferred in this regard, since the analogy of the infraorbital sinus and phylogenetic evaluations between the lovebird (*A. roseicollis*) and other parrots was impossible.

Massari et al.(2020) performed CT on the head of a macaw and concluded that the infraorbital, periorbital, and rostral diverticulum of the infraorbital sinus can be easily detected, mainly due to the large chambers of this sinus and the absence of covering muscles in this region. It was further indicated that the postorbital, quadrate, and mandibular recess parts were not detectable because they were small and superimposed by the masticatory muscle. These results corroborate those of the present study. The results of the present study revealed that in the lovebird (*A. roseicollis*), except for the periorbital, transverse canal, and rostral diverticulum, the remaining parts of the suborbital sinus were covered by the masticatory muscle.

In some studies, the existence of a paratracheal recess was reported in the Amazon and Cockatoo (Carril et al., 2016), as well as in Anodorhynchus and Ararauna macaws (Monção-Silva et al., 2016). The results of these studies contradict those of the current study. Based on our observations, the paratracheal recess was not observed in any of the lovebirds under investigation; therefore, this feature can be mentioned in the comparative anatomy of this type of parrot.

The skull of the lovebird (*A. roseicollis*) was relatively small, and the distance between its constituent bones was visible. The periorbital sinus was located in the anterorbital fenestra, and the zygomatic process of the squamosal bone surrounded the postorbital sinus. In the CT images, the muscles of the head of this parrot were detected as hyperattenuated lines and were unclear. However, relatively larger muscles, such as the quadrate, pterygoid, and ethmomandibular were distinguishable. Although the jaw adductor muscle was large, it could not be detected in the CT images, and its boundaries was determined based on the topography of the bones in that region.

Based on the current study's results, the columella ossicle, external cartilage, and the cochlea were not recognizable in the CT images. This is mainly due to the small size. Hence, it is recommended that other diagnostic imaging methods, such as micro-CT or MRI, be utilized in cases where they are intended to evaluate these structures.

Analysis of the results and their comparison with the results of other studies revealed that the skull of the lovebird (*A. roseicollis*) was not significantly different from that of other parrots. The only morphological differences were related to some parts of the nasal cavity, the infraorbital sinus, and, to some extent, the hyobranchial apparatus and the nasopharyngeal duct.

Conclusion

Overall, CT is one of the most appropriate and valuable diagnostic imaging methods to describe and dissect most of the hard and soft tissues of the head of the lovebird (*A. roseicollis*). The results of this study demonstrated that CT images can be used to examine the infraorbital sinus, turbinate, or conchae of the nasal cavities. Investigation of the tomographic features of the head of the lovebird (*A. roseicollis*) can be useful in identifying anatomical features and evaluating pathological cases. This study investigated the normal anatomy of the lovebird (*A. roseicollis*) head by CT using 3D modeling. The simultaneous CT evaluation and anatomical examination of the head of the lovebird showed highly correlated findings. The research results can be used as a reference and atlas to identify anatomical characteristics, examine various species of lovebirds (*A. roseicollis*), teach anatomy, and interpret CT scan images. Moreover, they can be used for the clinical examination and treatment of this type of parrot.

Ethical Considerations

Compliance with ethical guidelines

This study was approved by the Ethics Committee of Urmia Branch, Islamic Azad University, Urmia, Iran (Code: IR.IAU.URMIA.REC.1403.038) and used procedures that did not differ from established internationally recognized high standards (best practice) of veterinary clinical care for individual animals.

Funding

The paper was extracted from the PhD dissertation of Maryam Azari, approved by Department of Clinical Sciences, Faculty of Veterinary Medicine, Urmia Branch, Islamic Azad University, Urmia, Iran. This study was financially supported by Urmia Branch, Islamic Azad University, Urmia, Iran (Code: 4/ 39822).

Authors' contributions

All authors contributed equally to the conception and design of the study, data collection and analysis, interpretation of the results, and drafting of the manuscript. Each author approved the final version of the manuscript for submission.

Conflict of interest

The authors declared no conflicts of interest.

Acknowledgments

The authors thank the Vice Chancellor for Research of Islamic Azad University of Urmia for their financial support.

References

Al-Rubaie, N. I., & Kadhim, K. (2023). Anatomical comparison of the nasal cavity in adult male and female cockatiel (Nymphicus Hollandicus). *Acta Biomed, 94*, 2023719. [Link]

Benedict, L., Charles, A., Brockington, A., & Dahlin, C. R. (2022). A survey of vocal mimicry in companion parrots. *Scientific Reports, 12*(1), 20271. [DOI:10.1038/s41598-022-24335-x] [PMID]

Brühschwein, A., Klever, J., Wilkinson, T., Jr, & Meyer-Lindenberg, A. (2018). DICOM standard conformance in veterinary medicine in Germany: A survey of imaging studies in referral cases. *Journal of Digital Imaging, 31*(1), 13–18. [DOI:10.1007/s10278-017-9998-x] [PMID]

Carril, J., Tambussi, C. P., Rasskin-Gutman, D. (2021). The network ontogeny of the parrot: Altriciality, dynamic skeletal assemblages, and the avian body plan. *Evolutionary Biology, 48*, 41-53. [DOI:10.1007/s11692-020-09522-w]

Carril, J., Tambussi, C. P., Degrange, F. J., Benitez Saldivar, M. J., & Picasso, M. B. (2016). Comparative brain morphology of Neotropical parrots (Aves, Psittaciformes) inferred from virtual 3D endocasts. *Journal of Anatomy, 229*(2), 239–251. [DOI:10.1111/joa.12325] [PMID]

Casteleyn, C., Cornillie, P., Van Cruchten, S., Van den Broeck, W., Van Ginneken, C., & Simoens, P. (2018). Anatomy of the upper respiratory tract in domestic birds, with emphasis on vocalization. *Anatomia, Histologia, Embryologia, 47*(2), 100–109. [DOI:10.1111/ahe.12336] [PMID]

Cubo, J. & Casinos, A. (2000). Incidence and mechanical significance of pneumatization in the long bones of birds. *Zoological Journal of the Linnean Society, 130*(4), 499-510. [DOI:10.1111/j.1096-3642.2000.tb02198.x]

Dueker, S., Willows-Munro, S., Perrin, M. R., Abebe, Y. D. & Mwangi, E. W. (2023). Conservation status and threats to lovebirds: knowledge gaps and research priorities. *Ostrich, 94*(1), 1-27. [DOI:10.2989/00306525.2023.2206674]

Duymus, M., Demiraslan, Y., Akbulut, Y., Orman, G., Aslan, K. & Ozcan, S. (2013). The statistical analysis of some volumetric measurements in the japanese quails' head with different feather color: A computed tomography study. *Journal of the Faculty of Veterinary Medicine Kafkas University, 19*(4), 681-6. [DOI:10.9775/kvfd.2013.8650]

Faillace, A. C. L., Vieira, K. R. A., & Santana, M. I. S. (2021). Computed tomographic and gross anatomy of the head of the blue-fronted Amazon parrot (Amazona aestiva). *Anatomia, Histologia, Embryologia, 50*(1), 192–205. [DOI:10.1111/ahe.12618] [PMID]

Faux, C. M. & Logsdon, M. L. (2022). Infraorbital sinusitis. In J. A. Orsini., N. S. Grenager., & A. de Lahunta (Eds.), *Comparative veterinary anatomy* (pp. 1264-1270). Amsterdam: Elsevier. [DOI:10.1016/B978-0-323-91015-6.00116-3]

Forouzan, P. & Cohen, P. R. (2021). Parrot Beak nail: Case report and review of parrot beak nail dystrophy. *Cureus, 13*(6), e15974. [DOI:10.7759/cureus.15974]

Grist, A. (2006). *Poultry inspection. Anatomy, Physiology and Disease Conditions*. New York: Context. [Link]

Hanafy B. G. (2021). Structural adaption of the nasal conchae of Eurasian common moorhen (Gallinula chloropus chloropus, Linnaeus, 1758)-Histomorphological study. *Microscopy Research and Technique, 84*(9), 2195–2202. [DOI:10.1002/jemt.23778] [PMID]

Hébert J. A. (2019). Closed reduction of a rostroparasphenopalatal luxation in a red-crowned parakeet (Cyanoramphus novaezelandiae). *Journal of Avian Medicine and Surgery, 33*(3), 285–288. [DOI:10.1647/1082-6742-33.3.285] [PMID]

Henley, E. (2018). A bird's eye view of breakdown in parrot-caregiver relations. *Companion Animal, 23*(2), 104-8. [DOI:10.12968/coan.2018.23.2.104]

Hollwarth, A. J., Esmans, M. C., Herrmann, A., & Dutton, T. A. G. (2023). Heterotopic ossification bone formation in the frontal bones of an African grey parrot (Psittacus erithacus). *Journal of Avian Medicine and Surgery, 36*(4), 388–393. [DOI:10.1647/22-00002] [PMID]

Isabelle, L., Vanessa, B. R., & Philippe, D. J. (2020). Rhinitis due to Aspergillus pseudoviridinutans in an orange-winged Amazon parrot (Amazona amazonica). *Medical Mycology Case Reports, 30*, 46–50. [DOI:10.1016/j.mmcr.2020.11.001] [PMID]

Iwaniuk, A. N., Dean, K. M., & Nelson, J. E. (2005). Interspecific allometry of the brain and brain regions in parrots (psittaciformes): Comparisons with other birds and primates. *Brain, Behavior and Evolution, 65*(1), 40–59. [DOI:10.1159/000081110] [PMID]

Jones, M. E. H., Button, D. J., Barrett, P. M., & Porro, L. B. (2019). Digital dissection of the head of the rock dove (Columba livia) using contrast-enhanced computed tomography. *Zoological letters, 5*, 17. [DOI:10.1186/s40851-019-0129-z] [PMID]

Krautwald-Junghanns, M. E., Kostka, V. M., & Dörsch, B. (1998). Comparative studies on the diagnostic value of conventional radiography and computed tomography in evaluating the heads of psittacine and raptorial birds. *Journal of Avian Medicine and Surgery, 12*(3), 149-157. [Link]

Langlois, I., Barrs, V. R. & Dufresne, P. J. (2020). Rhinitis due to Aspergillus pseudoviridinutans in an orange-winged Amazon parrot (Amazona amazonica). *Medical Mycology Case Reports, 30*, 46-50. [DOI:10.1016/j.mmcr.2020.11.001] [PMID]

Ma, S., Wang, L., Liu, Z., Luo, X., Zhou, Z., & Xie, J., et al. (2021). One stone, two birds": Engineering 2-D ultrathin heterostructure nanosheet BiNS@NaLnF4 for dual-modal computed tomography/magnetic resonance imaging guided, photonic synergetic theranostics. *Nanoscale, 13*(1), 185–194. [DOI:10.1039/D0NR07590F] [PMID]

Madkour, F. (2019). Anatomical descriptions of the nasal cavity of the aquatic and non-aquatic birds. *SVU-International Journal of Veterinary Sciences, 2*(2), 101-10. [DOI:10.21608/svu.2019.14982.1022]

Marez, C. (2003). The Abyssinian Lovebird. *AFA Watchbird, 30*(3), 20-3. [Link]

Massari, C. H. d. A. L., Silva, A. F., Magalhães, H. I. R., Silva, D. R. S., Sasahara T. H. d. C. & Miglino, M. A. (2020). Anatomía comparada de los picos de guacamayo azul y amarillo (Ara ararauna) y de tucán toco (Ramphastos toco) mediante análisis macroscópico y tomografía computarizada. *International Journal of Morphology, 38*(6), 1591-6. [DOI:10.4067/S0717-95022020000601591]

Mohammed, F., Baydaa Abed Hussein, A., & Ahmed, T. (2022). Evaluation of methylation panel in the promoter region of p16INK4a, RASSF1A, and MGMT as a biomarker in sputum for lung cancer. *Archives of Razi Institute, 77*(3), 1075–1081. [DOI:10.22092/ARI.2022.357985.2131] [PMID]

Monção-Silva, R. M., Ofri, R., Raposo, A. C. S., Libório, F. A., Estrela-Lima, A. & Oriá, A. P. (2016). Ophthalmic parameters of Blue-and-yellow Macaws (Ara ararauna) and Lear's Macaws (Anodorhynchus leari). *Avian Biology Research, 9*(4), 240-9. [DOI:10.3184/175815516X14725499175746]

Moore, B. A., Oriá, A. P. & Montiani-Ferreira, F. (2022). Ophthalmology of psittaciformes: Parrots and relatives. In F. Montiani-Ferreira., B. A. Moore., Ben-Shlomo, G (Eds.), *Wild and exotic animal ophthalmology: Volume 1: Invertebrates, fishes, amphibians, reptiles, and birds* (pp. 349-391). Berlin: Springer. [DOI:10.1007/978-3-030-71302-7_17]

Orosz, S. (2016). Clinical respiratory anatomy.Paper presented at: NAVC Conference 2016, Orlando, United States, 20 January 2016. [Link]

Pavlova, T. V., Pilkevich, N. B., Bessmertnyi, D. V., Pavlov, I. A., Atiakshin, D. V., & Pavlova, L. A. (2021). Evaluation of new immunohistochemical approaches for the study of kidney tumors in geriatric. *Archives of Razi Institute, 76*(4), 1107–1113. [DOI:10.22092/ari.2021.355858.1731] [PMID]

Piro, A. & Acosta Hospitaleche, C. (2019). Skull anatomy of Wilson's storm-petrel Oceanites oceanicus (Hydrobatidae, Procellariiformes). *Polar Biology, 42*(8), 1501-10. [DOI:10.1007/s00300-019-02536-x]

Rassouli, M., Oliya Ardekani, A., & Moazzezi, H. (2022). Hadjelia truncata infection among quails (Coturnix coturnix) in Semnan City, Iran. *Iranian Journal of Veterinary Medicine, 18*(3), 459-464. [DOI:10.32598/ijvm.18.3.1005302]

Sabat, D., Millan, S., Suchismita Sethy, P., Marathe, S., Sahoo, H., Mishra, M. & editors. (2017). Elemental analysis of various feathers of Indian rose ringed parakeet psittacula krameri. paper presented at: 3rd International Multidisciplinary Microscopy and Microanalysis Congress (InterM) Proceedings, Oludeniz, Turkey, 10 November 2016. [DOI:10.1007/978-3-319-46601-9_5]

Salavati, A., Peighambari, S. M., Yazdani, A., & Razmyar, J. (2024). The relative frequency of histomonas meleagridis infection in Turkey flocks in some provinces of Iran. *Iranian Journal of Veterinary Medicine, 18*(3), 387-396. [DOI:10.32598/IJVM.18.3.1005384]

Salehi, F., Partovi, R., & Seifi, S. (2024). [Effect of dietary supplementation of silybum marianum and artichoke (Cynara scolymus L.) on Japanese quail's carcass characteristics, oxidative stability, and quality of breast meat (Persian)]. *Iranian Journal of Veterinary Medicine, 18*(1), 87-96. [DOI:10.32598/IJVM.18.1.1005318]

Silva, I. A., Vieira, L. C., Mancini, V. R. M., Faillace, A. C. L., & Santana, M. I. S. (2020). Radiographic anatomy of the cockatiel (Nymphicus hollandicus) axial and appendicular skeleton. *Anatomia, Histologia, Embryologia, 49*(2), 184–195. [DOI:10.1111/ahe.12510] [PMID]

Silveira, R., Almeida, J. & Alves, M. (2023). Rosy-faced lovebirds', Agapornis roseicollis (Aves: Psittaciformes), response to their own image reveals self-recognition behaviour. *Behaviour, 160*(10), 889-909. [DOI:10.1163/1568539X-bja10238]

Šljivic, M., Pavlovic, A., Kraišnik, M., & Ilić, J. (2019). Comparing the accuracy of 3D slicer software in printed enduse parts. Paper presented at: IOP conference series: Materials science and engineering, Kazimierz Dolny, Poland, 23 November 2019. [DOI:10.1088/1757-899X/659/1/012082]

Smallwood, J. E. (2014). *A guided tour of avian anatomy*. Morrisville: Millennium Pring Group. [Link]

Stevens, A., Doneley, R., Cogny, A., & Phillips, C. J. (2021). The effects of environmental enrichment on the behaviour of cockatiels (Nymphicus hollandicus) in aviaries. *Applied Animal Behaviour Science, 235*, 105-154. [DOI:10.1016/j.applanim.2020.105154]

Thurber, M. I., Mans, C., Fazio, C., Waller, K., Rylander, H., & Pinkerton, M. E. (2015). Antemortem diagnosis of hydrocephalus in two Congo African grey parrots (Psittacus erithacus erithacus) by means of computed tomography. *Journal of the American Veterinary Medical Association, 246*(7), 770–776. [DOI:10.2460/javma.246.7.770] [PMID]

Van Zeeland, Y. (2018). Upper respiratory tract disease. In J. Chitty., & D. Monks (Eds.), *BSAVA manual of avian practice* (pp. 299-316). Gloucester: British Small Animal Veterinary Association. [DOI:10.22233/9781910443323.20]

Vučićević, M., Stevanović, J., Šekler, M., Resanović, R. & Stanimirović, Z. (2016). Historical overview of methods for sex determination in birds. *Veterinarski Glasnik, 70*, 145-57. [DOI:10.2298/VETGL1604145V]

Webb, T. J., & Gaston, K. J. (2000). Geographic range size and evolutionary age in birds. Proceedings. *Biological Sciences, 267*(1455), 1843–1850. [DOI:10.1098/rspb.2000.1219] [PMID]

Wild, J. M. (2015). The avian somatosensory system: a comparative view. In C. G. Scanes (Ed.), Sturkie's avian physiology (pp. 55-69). Amsterdam: Elsevier. [DOI:10.1016/B978-0-12-407160-5.00005-1]

Wilhite, R., & Wölfel, I. (2019). 3D Printing for veterinary anatomy: An overview. *Anatomia, Histologia, Embryologia, 48*(6), 609–620. [DOI:10.1111/ahe.12502] [PMID]

Yaren, Kuloğlu., H., & Boydak, M. (2024). [A periodic comparison of harderian gland in henna partridge (Alectoris chukar) according to different developmental stages (Persian)]. *Iranian Journal of Veterinary Medicine, 18*(3), 359-376. [DOI:10.32598/IJVM.18.3.1005521]

Yokosuka, M., Hagiwara, A., Saito, T. R., Aoyama, M., Ichikawa, M., & Sugita, S. (2009). Morphological and histochemical study of the nasal cavity and fused olfactory bulb of the brown-eared bulbul, Hysipetes amaurotis. *Zoological Science, 26*(10), 713–721. [DOI:10.2108/zsj.26.713] [PMID]